Earthquakes and Structures, *Vol. 15, No. 6 (2018) 655-665*
DOI: https://doi.org/10.12989/eas.2018.15.6.655

Use of large-scale shake table tests to assess the seismic response of a tunnel embedded in compacted sand

Hao Zhou[1a], Xiaoyang Qin[2b], Xinghua Wang[*1] and Yan Liang[1c]

[1]*Department of Civil Engineering, Central South University, Changsha 410075, China*
[2]*Department of Civil and Environmental Engineering, University of Auckland, New Zealand*

(Received April 24, 2018, Revised July 23, 2018, Accepted November 9, 2018)

Abstract. Shield tunnels are widely used throughout the world. However, their seismic performance has not been well studied. This paper focuses on the seismic response of a large scale model tunnel in compacted sand. A 9.3 m long, 3.7 m wide and 2.5 m high rigid box was filled with sand so as to simulate the sandy soil surrounding the tunnel. The setup was excited on a large-scale shake table. The model tunnel used was a 1:8 scaled model with a cross-sectional diameter of 900 mm. The effective shock absorbing layer (SAL) on the seismic response of the model tunnel was also investigated. The thickness of the tunnel lining is 60 mm. The earthquake motion recorded from the Kobe earthquake waves was used. The ground motions were scaled to have the same peak accelerations. A total of three peak accelerations were considered (i.e., 0.1 g, 0.2 g and 0.4 g). During the tests, the strain, acceleration and soil pressure on the surface of the tunnel were measured. In order to investigate the effect of shock absorbing layer on the dynamic response of the sand- tunnel system, two tunnel models were set up, one with and one without the shock absorbing layer of foam board were used. The results shows the longitudinal direction acceleration of the model tunnel with a shock absorbing layer were lower than those of model tunnel without the shock absorbing layer, Which indicates that the shock absorbing layer has a beneficial effect on the acceleration reduction. In addition, the shock absorbing layer has influence on the hoop strain and earth pressure of the model tunnel, this the effect of shock absorbing layer to the model tunnel will be discussed in the paper.

Keywords: large-scale model tunnel; double shake table test; dynamic soil pressure; shock absorbing layer

1. Introduction

It is commonly perceived that tunnels have a better seismic performance than above-ground structures during earthquakes. However, recent earthquakes showed that some underground structures were serious damaged under strong earthquakes. For example, the collapse of the Daikai subway metro station in Japan during the 1995 Kobe earthquake (Hassan *et al*. 2009a, b), the failure of the Bolu tunnel in the 1999 İzmit earthquake (Giannakou *et al*. 2005a, b), and the damage of the Long Xi tunnel in China during the 2008 Wen Chuan earthquake Shen (2014). These failures revealed that the current practices of seismic design for underground structures cannot ensure the seismic performance of tunneling structures. Therefore, how to improve safety of tunnels during earthquakes has become one of the major concerns for the engineering.

An increasing number of studies have been conducted to investigate the dynamic response of tunnels subjected to earthquake loading. The main approach is through theoretical analysis, such as uncoupled methods, simplified closed-form solutions, equivalent static analyses, and coupled soil-structure interactions incorporating advanced numerical methods (i.e., Wang 1993, Penzien 2000, Hashash *et al*. 2001a, b, ISO23469 2005, Abuhajar *et al*. 2015a, b, Zhou *et al*. 2016a, b). However, the accuracy of these approaches have not been validated. For the same system, the response of tunnel estimated using different approach can be significantly different.

Experimental tests on physical model could also help to study the seismic behavior of tunnels. These experiments used seismic wave from earthquake or an artificial wave to excite a physical tunnel model to simulate the dynamic response of tunnel under earthquake (Jiang *et al*. 2010a, b, Cilingir and Madabhushi 2011, Tsinidis *et al*. 2014a, b, 2015a, b, Lanzano *et al*. 2012a, b). But most of the previous studies are presented the experimental data to reflect the dynamic response of tunnels without the shock absorbing layer. However, to date, seismic isolation has been used successfully in above-ground structures ((Tavakoil *et al*. 2015a, b, Vasiliadis 2016, Patil *et al*. 2016a, b, Hessabi *et al*. 2017a, b, Milanchian *et al*. 2017a, b, Wei *et al*. 2017a, b). Only a few researchers have studied the effect of shock absorbing layer with numerical simulation (Kusakabe *et al*. 2008a, b, Yamada *et al*. 2004a, b) and small scale model tests Chen and Shen (2014). According to the Saint-Venant principle. These small scale model tests can oversimplify

∗Corresponding author, Professor
E-mail: xhwang@mail.csu.edu.cn
[a]Ph.D. Student
E-mail: haozhou@csu.edu.cn
[b]Ph.D.
E-mail: xqin009@aucklanduni.ac.nz
[c]Ph.D. Student
E-mail: liangyan19850308@163.com

ISSN: 2092-7614 (Print), 2092-7622 (Online)

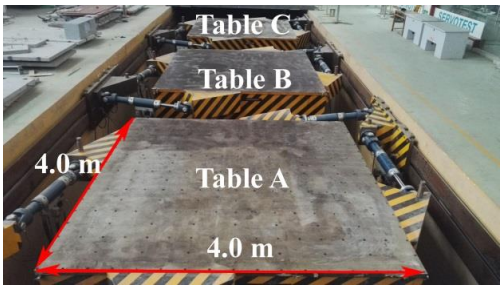

(a) Three tables and horizontal actuators

(b) Vertical actuators

Fig. 1 Laboratory multi-function shaking table system

the complexity of the detail and response characteristic of a tunnel structure. It is even more difficult to show the realistic response to the lining force and failure characteristics of the tunnel. Moreover, Andrew (1997) found that as the difference in the scales of the model and prototype increases, the difference in the three-dimensional and time varying properties also increases. Therefore, based on reducing the difference brought by the small scale and the influence of boundary effects, in order to investigate the dynamic response of a tunnel and the soil-tunnel interaction, it is necessary to carry out the shake table test of large-scale (1:8) shield tunneling models in 9.3 m long, 3.7 m wide and 2.5 m high rigid box.

The objectives of this study are: (a) to provide experimental data on the seismic response of circular tunnels in compacted sand under earthquake motions and sinusoidal wavelets; (b) to determine the differences in the measured accelerations, strains and dynamic earth pressures between the cross-sections with and without a shock absorbing layer (SAL); (c) to evaluate the efficiency of the SAL during earthquake loadings. In this paper, the series of shake table tests on large-scaled circular model tunnels embedded in dry sand are presented first. The tests have been conducted at the Shaking Table Laboratory of the National Engineering Laboratory for Construction Technology of High Speed Rail in Central South University, China. Following a detailed description of the experimental setup, a detail description of the experimental setup is provided, focusing on the design of the model casing, sand used in the tests and the scaled tunnel liner model, instrumentation and test procedure. The main experimental data obtained from the tests are summarized and discussed in terms of the concrete strain, dynamic earth pressure, acceleration and frequency. Hence, the experimental data can be used to better understand the seismic behavior of circular tunnels and to improve seismic design methods for tunnels.

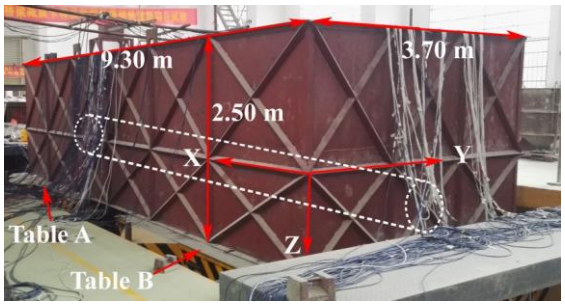

Fig. 2 Soil container

2. Test setup and model preparation

2.1 Shake table system

The shake table tests were performed using the Laboratory Multi-Function Shaking Table System (LMSTS) in the National Engineering Laboratory of High Speed Railway Construction Technology in Central South University, China. The LMSTS has an electro-hydraulic servo drive. The system consists of three 4 m×4 m 6-DOF mobile stations, which can be controlled independently to simulate single or multiple three-directional ground motions. It was built in 2009 and equipped with advanced instruments for high-performance dynamic signal acquisition, which can carry out independent sampling of 320 input channels for accelerometers, strain gauges and earth pressure sensors. Fig. 1 shows the layout of LMSTS and the horizontal and vertical actuators. For the tests conducted in this study, only Tables A and B were used.

2.2 Soil container

The soil container is a rigid box with overall dimensions of 9.30 m long (x), 3.70 m wide (y) and 2.50 m high (z) as shown in Fig. 2. The container consists of three parts: (a) steel plates, (b) inner framework, and (c) outer framework. Steel plates of 6 mm in thickness were used to form the box wall. The inner framework consists of steel strips welded onto the box wall to ensure the box is rigid (Fig. 2); the outer framework consists of angle steels welded between steel plates. Two transverse ribs were welded onto the top of the model container. The bottom of the box is a 5 mm thick steel plate welded on to the frame. The inner bottom of the box was divided into 1.0 m^2 baffle plates using welded angle steels. The total weight of the empty box is approximately 3,800 kg. The rigid box was bolted firmly onto Tables A and B using a total of 64 high-strength bolts. The length/height ratio of the container is 3.72, which is more than 3 and designed to reduce the boundary effect of the rigid end wall (Whitman *et al*. 1986a, b) and (Fishman *et al*. 1995a, b).

To mimic the free-field boundary condition, flexible materials are generally installed inside the rigid container to reduce the boundary effect of the box wall during shake table tests (Mizuno and Iiba 1984, Lombardi *et al*. 2015a, b). These flexible materials are usually polystyrene foam boards and sponge rubber and are used to create a wave-absorbing boundary condition (Ha *et al*. 2012a, b,

Table 1 Similarity ratios of the model to prototype.

Physical parameter	Similarity relationship	Similarity ratio
Geometry	C_l	1/8
Density	C_ρ	4/5
Elastic module	C_E	1/10
Strain	C_ε	1
Stress	$C_\sigma = C_E \times C_\varepsilon$	1/10
Acceleration	C_a	1
Poisson's ratio	C_ν	1
Friction angle	Φ	1
Frequency	$C_f = C_l^{-1}(C_E / C_\rho)^{1/2}$	2.828
Time	$C_t = C_l^{1/2}$	0.354

Bhattacharya *et al*. 2011a, b) In this study, a 10 cm thick polystyrene foam board was attached to the container walls; in addition, a 5 cm thick and a 2.5 cm thick sponge rubber boards were attached to the end walls and the side walls, respectively. At the bottom of the model box, a layer of 2-3 cm diameter aggregate was placed to increase the frictional resistance between the model soil and the floor to reduce potential slippage.

2.3 Tunnel model and materials

The model tunnel is scaled at 1:8. Similarity law was developed to obtain the scaled factors of the experiment. The theory is well documented for a wide range of engineering applications Qin (2016). A set of dimensionless variables was developed. By matching the corresponding dimensionless variables of the scaled model with the prototype, the scale factor for each physical variable can be determined by Qin and Chouw (2017, 2018). The dimensionless group for tunnel structure in soil has been studied by Victor (2010). Table 1 summarizes the considered physical variables. It should be noted that the scaling law is only valid for scaling a system with linear behavior, while in this work three nonlinearities were considered. Thus the experimental measurements may not be able to precisely replicate the response of the prototype. However, the results obtained can still provide a useful indication of the performance of the prototype. The prototype tunnel has a cross-sectional diameter of 7200 mm and a lining thickness of 480 mm. According to the similarity law (David *et al*. 2002a, b), the cross-sectional diameter of the model tunnel is therefore 900 mm and the thickness of the tunnel lining is 60 mm. Table 1 shows the similarity ratios of the model.

Natural sand from the Xiangjiang River was used to form the soil deposit around the model tunnel. Fig. 3 shows the grain size distribution of the sand, which can be classified as SP according to the Unified Soil Classification System. The sand was placed into the rigid box and was compacted in lifts of 10 cm thick with 50 kg regular weight to tamper five times to a relative density of 63%. The water content of sand is 4.9% which is belong to dry sand to a relative density of 63%. Table 2 shows the physical properties of the compacted sand.

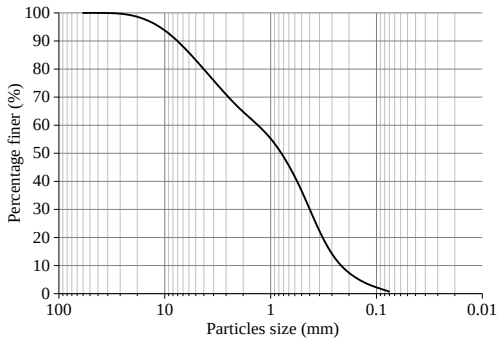

Fig. 3 Grain size distribution of sand

Table 2 Physical properties of sand

Dry density(g/cm^3)	Cohesion (kPa)	Internal friction angle (°)	Water content (%)	Poisson's ratio
1.64	1.5	28.6	4.90	0.243

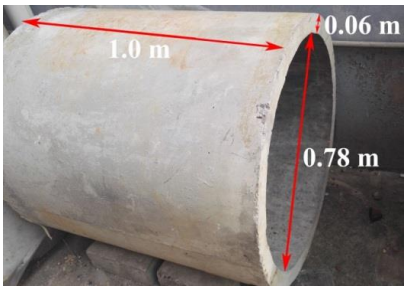

Fig. 4 Model tunnel

Table 3 Mechanical properties of model tunnel

Density ρ_t (kg/m^3)	Elastic modulus E_t (GPa)	Poisson's ratio, ν_t	Yield strength f_t (MPa)
1900	3	0.23	6

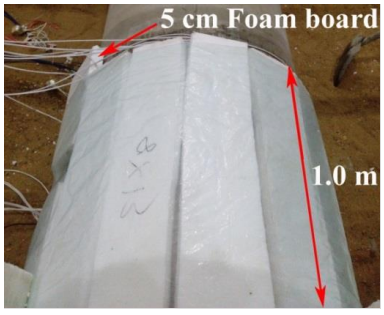

Fig. 5 Shock absorbing layer (SAL)

As shown in Fig. 4, On the basis of equivalent stiffness principle, the tunnel lining is made of micro-concrete with an inside diameter of 0.78 m and a thickness of 0.06 m. It is reinforced with 6 mm diameter steel mesh at the radial ring spacing of 10 mm. Table 3 shows the typical mechanical properties of the lining used in the tests. A 5 cm thick foam board was used to wrap a section of the model tunnel (see Fig. 5) to investigate the effect of the SAL on the tunnel response under seismic shaking. Previous dynamic finite difference method reveal 5 cm thick foam board can significantly reduce the seismic dynamic response of the second lining of tunnels. The shake table tests also reveal

Table 4 Mechanical properties of foam board

Density ρ_t (kg/m^3)	Elastic modulus E_t (kPa)	Poisson's ratio, ν_t	Damping ξ (%)
12	16	0.29	24

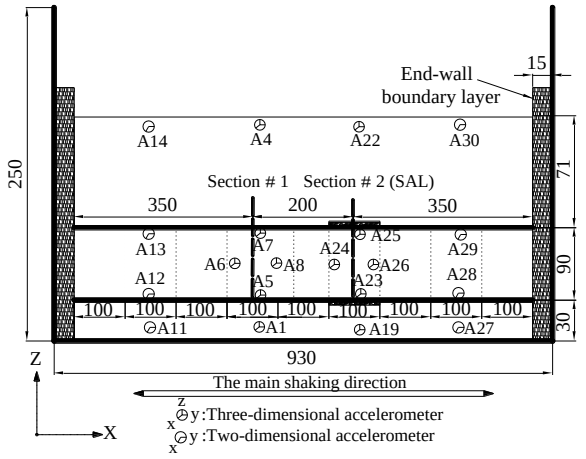

(a) Profile layout

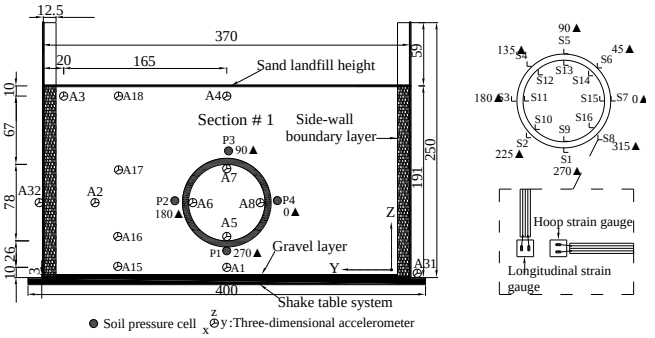

(b) Cross-section # 1 layout of sensors

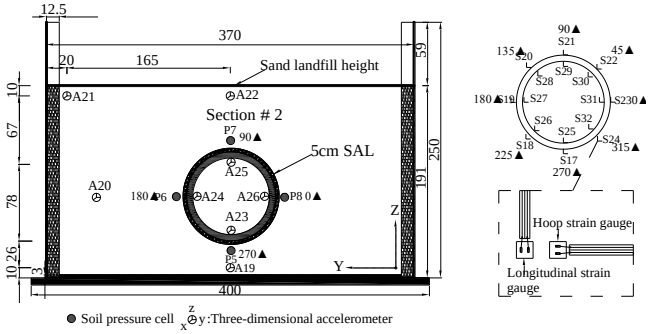

(c) Cross-section # 2 layout of sensors

Fig. 6 Instrumentation layout (Unit: cm)

that the strains of lining are reduced by the SAL (Yamada *et al*. 2004a, b, Shen *et al*. 2014a, b). Table 4 shows the mechanical properties of the foam board.

2.4 Instrumentation

Various sensors have been instrumented to monitor the model response and Fig. 6 shows the instrumentation layout.

As shown in Fig. 6(a), there are two main cross-sections designed for monitoring in the model container. One is the cross-section # 1, the other is the cross-section # 2 with a 5 cm thick foam board wrapping the tunnel lining. As shown in Figs. 6(b)-(c)), three sets of transducers have been installed in the rigid box. One set of accelerometers to measure the accelerations in the *X*, *Y* and *Z* directions at the base of the tunnel lining. Another set to measure the accelerations at the base of the rigid box, and a third set to measure the accelerations on the shake table. As shown in Fig. 6(a), dynamic earth pressure cells have been used to measure the earth pressure at the interface of the sand. As shown in Figs. 6(b)-(c)), strain gauges have been used to measure the deformation of the inner and outer surfaces of the tunnel lining.

2.5 Experimental program and test procedure

During the tests, white noise and harmonic motions frequency sweeps and the recorded earthquake input motions were used. White noise sweep can determine the approximate range of the natural frequency of the model casing. Harmonic motions sweep can accurately confirm the natural frequency of the model casing. In order to prevent any adverse effect of damage accumulation on the test results, the sweep motion tests of white noise and harmonic motions have been conducted with 0.05 g peak accelerations only. The results of the tests are as follows. The natural frequency of the empty model container in the *X*-direction is 35.31 Hz. However, the natural frequency of the sand in the model in the *X*-direction is 3.82 Hz. This is an indication that the shear stiffness of the model container is much higher than that of the sand in the model, which can prevent the resonance effect between the model box and the sand during the test.

Earthquake records have been used as input motions in the shake table tests. There is the Kobe earthquake measured in 1995 at the OKA Station. The geological conditions of Kobe earthquakes are similar and the records have been extracted from the PEER Strong Motion Database. For the input motions to the model, the duration and frequency of the earthquake records have been scaled by a factor of eight, as shown in Fig. 7. The input motions have been scaled up to different peak accelerations during the testing program. Three peak accelerations have been used (i.e., 0.1 g, 0.2, and 0.4 g), as shown in Table 5. There are two different loading condition, one is one- direction earthquake wave (i.e., EQ1, EQ3), which were used to demonstrate the reliability of the tests. The other is three-direction earthquake wave (i.e., EQ2, EQ4, EQ5), which were used to investigate the dynamic response of model tunnel.

Table 5 Characteristics of input motions

Test Event	Direction	Peak acceleration/g		
		X	*Y*	*Z*
EQ1	One-direction	0.1	/	/
EQ2	Three-direction	0.1	0.085	0.065
EQ3	One-direction	0.2	/	/
EQ4	Three-direction	0.2	0.17	0.13
EQ5	Three -direction	0.4	0.36	0.26

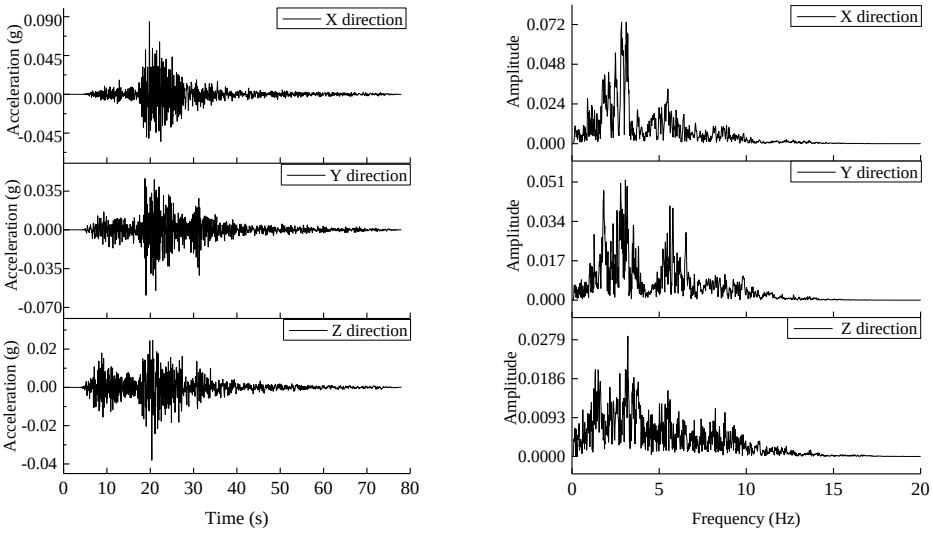

Fig. 7 Acceleration time history and frequency spectrum of the records Kobe earthquakes

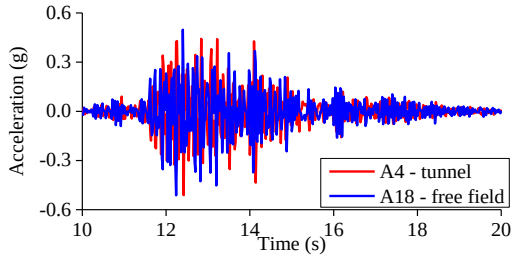

(a) Acceleration time history of the A4 and A18

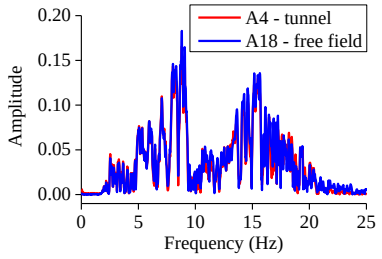

(b) Frequency spectrum of the A4 and A18

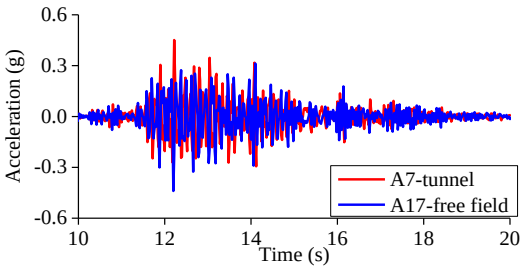

(c) Acceleration time history of the A7 and A17

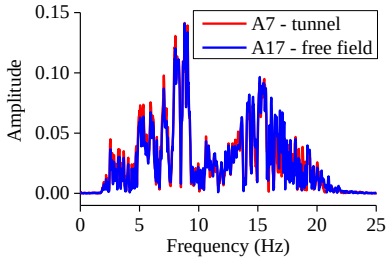

(d) Frequency spectrum of the A7 and A17

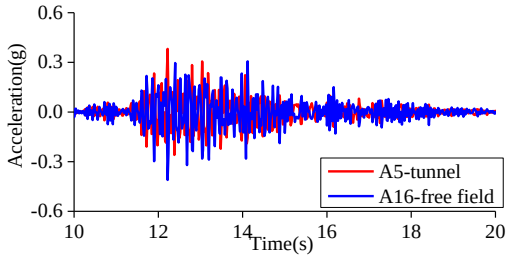

(e) Acceleration time history of the A5 and A16

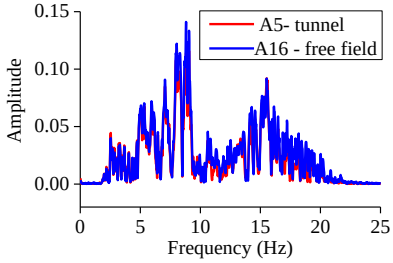

(f) Frequency spectrum of the A5 and A16

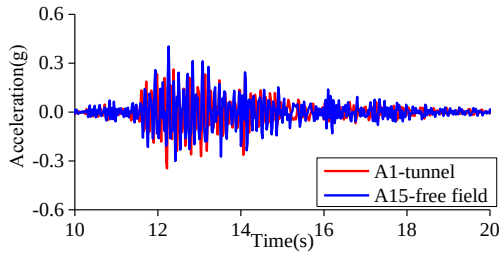

(g) Acceleration time history of the A1 and A15

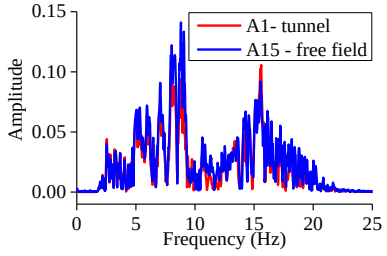

(h) Frequency spectrum of the A1 and A15

Fig. 8 Comparison between the results of model tunnel and the surrounding soil

3. Test results and discussion

3.1 Acceleration time histories

Fig. 8 shows the time histories and the Fourier spectra of the acceleration in the *X* direction different location of the tunnel Section # 1 (i.e., A4, A7, A5 and A1 in Fig. 6(b)) and that at the surrounding soil with the same depth (i.e., A18, A17, A16 and A15 in Fig. 6(b)) under EQ5 excitation. It is apparent that the range of domain frequency for the acceleration is 5-10 Hz. Comparing the amplitude of the domain frequency of tunnel and that of the surrounding soil, the amplitude of the soil at the position of A15 and A16 was significantly greater than the tunnel, while the opposite can be observed for the position of A17.

For comparison, all of the acceleration time histories have been "zero-centered" by scaling them with respect to the drift baseline. The frequency filter is a fourth-order Butterworth type (SeismoSignal Soft), which is an infinite impulse-response filter (IIR) acting as a typical "bandpass" between the frequencies of 0.1 Hz and 25 Hz. This filter has been used to eliminate the lowest and the highest frequencies, with the former typically associated to the drift of an accelerometer signal and the latter attributed to the electrical noise of recording. Further details on the signal processing can be found in Lanzano (2009), Lanzano *et al*. (2012a, b).

3.2 Profiles of peak acceleration with depth

The maximum accelerations of the acceleration time history have been determined and used as the maximum values of the semi-amplitude in the acceleration time histories. The profiles of these maximum accelerations from the base of soil container to the surface of the sand (i.e., Sensors A1, A5, A7, and A4) are shown in Fig. 9.

Fig. 9 shows the profiles of the maximum horizontal acceleration in the *X* direction with model tunnel and the surrounding soil for events EQ2, EQ4 and EQ5. It can be seen that the maximum accelerations increases gradually from base of soil container to 191 cm below surface in "free field" vertical array. However, with a model tunnel the maximum acceleration firstly decreases from the shake table to the base of soil container, then, these accelerations gradually increases from the bottom of model tunnel to ground surface of the sand in the model tunnel array, but then a remarkable increase in acceleration take place from the bottom to the crown of model tunnel compared to the same depth "free field" Because the weight of the model tunnel is about 300 kg that influence the sand below the bottom of model tunnel, what's more, the damping of wave propagation in the macro concrete is lower than the sand.

The results for excitation EQ2, EQ4 and EQ5 are summarized in Fig. 10, where they are plotted in terms of the ratio between the peak accelerations measured by from the base to the surface of sand for vertical array of the tunnel and the surrounding soil. This ratio is the conventional amplification factor and can be used to investigate the influence of the tunnel on the vertical propagation of shear waves. As shown in Fig. 10, the amplification factor at the base of soil container (A1) in

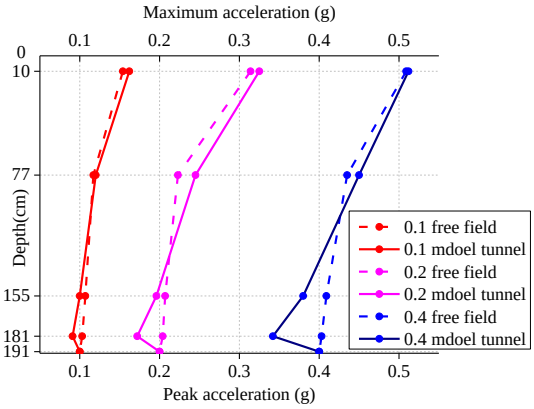

Fig. 9 Profiles of maximum horizontal acceleration with the Kobe wave excitation

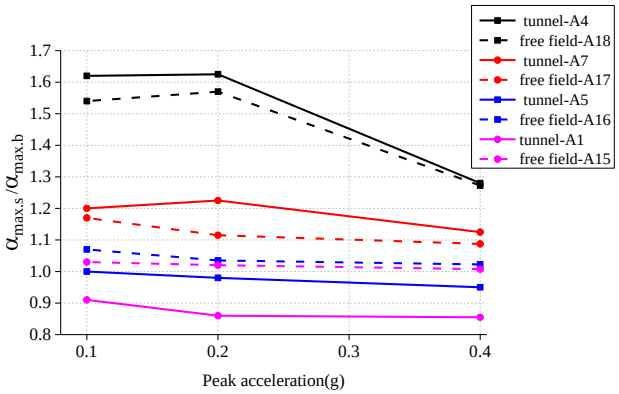

Fig. 10 Amplification factor of horizontal acceleration with different position

tunnel vertical array is lower than unity for all earthquakes, compared with same position (A15) in "free field" vertical array, which was attributed to the influence of large-scale model tunnel. The amplification factor at the bottom of model tunnel also is lower than unity, while the amplification factor at the crown of model tunnel (A7) is larger than the same position (A17) in the surrounding soil, This could be an explanation for the non-uniformity behavior of the sand, which is due to the arching effects, as well as the influence of the cavity boundary, reflecting down some of the shear waves propagating upward.

3.3 Effect of SAL on tunnel acceleration

Fig. 11 shows a comparison of the model tunnel section # 1 and section # 2, in the *X* direction, at different depth. It can be seen that the same phenomenon happened that the maximum acceleration firstly decreases from the shake table to the bottom of model tunnel, then, these accelerations gradually increases from the bottom of model tunnel to ground surface of the sand in the model tunnel array of section # 2. It is interesting that the point of minimum acceleration is located at the bottom of model tunnel with SAL. With the SAL are generally lower than those of the tunnel without. With increasing earthquake intensity, the reductions due to the SAL were larger. On the other hand, the peak acceleration at the soil above the

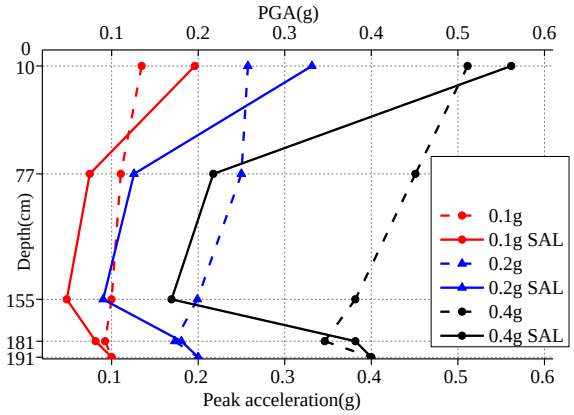

Fig. 11 Comparison of Kobe motion peak acceleration profiles with and without the SAL

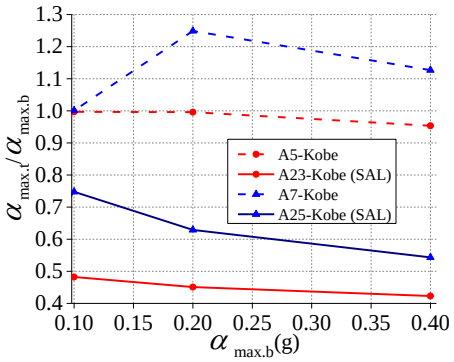

Fig. 12 Comparison of Kobe motion amplification factor

tunnel (i.e., location A4) was increased. The maximum accelerations at the crown and at the bottom (i.e., location A23 and A25) of the model tunnel with the SAL are generally lower than those of the model tunnel without.

Fig. 12 shows the amplification factor between the peak acceleration of the input excitation ($a_{max,b}$) and the maximum model tunnel acceleration ($a_{max,t}$). It can be seen that at the bottom (at location A23) and at the crown (at location A25) of the model tunnel, the amplification factor for the tunnel with the SAL are clearly smaller than one. It can also be seen that there is a tendency for the peak acceleration of the tunnel to attenuate from the bottom to the crown of model tunnel with the SAL. It has been shown that the peak accelerations at the crown and the bottom of the tunnel with SAL are always lower than those of the tunnel without SAL. This shows that the foam board has positive effect on the reduction of the acceleration.

Fig. 13 shows the acceleration reduction factor due to the SAL under different seismic loads. The calculation of the reduction factor is shown in Eq. (1), the reduction factor of the SAL with different peak acceleration of input motions. It can be seen that with small peak accelerations, the reduction factor of the SAL at the bottom of model tunnel is larger compared to the crown of model tunnel. However, as the peak accelerations of input motion increases (i.e., 0.2 g and 0.4 g), the reduction factor of the SAL at the crown of model tunnel is higher than that the bottom of model tunnel and more than 50%, which means the SAL can at least decreases the half accelerations of the

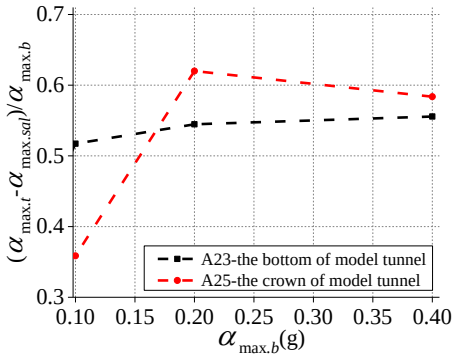

Fig. 13 SAL reduction factor

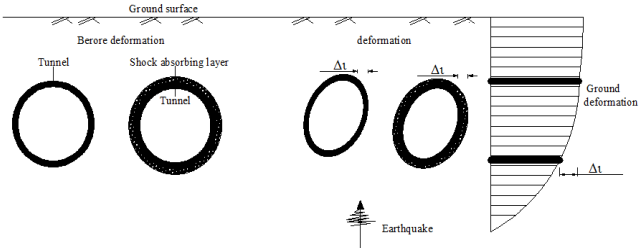

Fig. 14 Mechanism of the SAL

model tunnel without SAL.

$$\text{reduction factor} = \frac{\left(a_{max.t} - a_{max.sal}\right)}{a_{max.b}} \quad (1)$$

α_{max} is the maximum acceleration of model tunnel with SAL and without;

$\alpha_{max.t}$ is the maximum acceleration of model tunnel without SAL;

$\alpha_{max.sal}$ is the maximum acceleration of model tunnel with SAL;

$\alpha_{max.b}$ is the maximum acceleration of shaking table;

3.4 Tunnel deformation

Because of the variation of soil deformation over the depth, the deformation alone the cross-section of the tunnel also changes (as shown in Fig.14).

As discussed in section 2.4, for all experiments, the strains developed at different locations of the tunnel specimen were derived from the strains measured using the strain gauges. Fig. 15 shows the longitudinal and hoop strain time histories of the outer surfaces of model tunnel for events EQ1, EQ3. While EQ1 and EQ3 were excited the tunnel model in the *X* direction.

Fig. 15 presents the time history of the longitudinal and hoop strain at five different positions of the model tunnel. In theory, in the *X* direction excitation has only an effect on the longitudinal strain, For the *X* direction excitation with different intensity of earthquake waves were considered. As shown, the longitudinal strains developed at different locations of the tunnel are larger than the hoop strains. The result has evidenced that the shaking table tests for the model tunnel is reliable comparative analysis of the longitudinal and hoop strain.

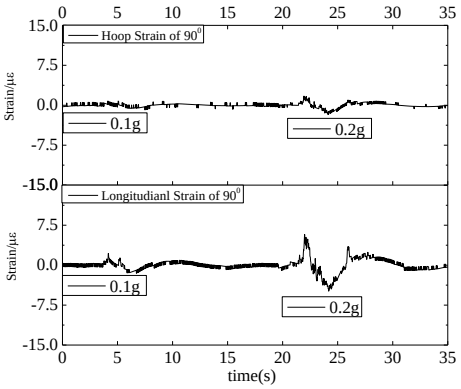

(a) hoop and longitudinal strain in 90°

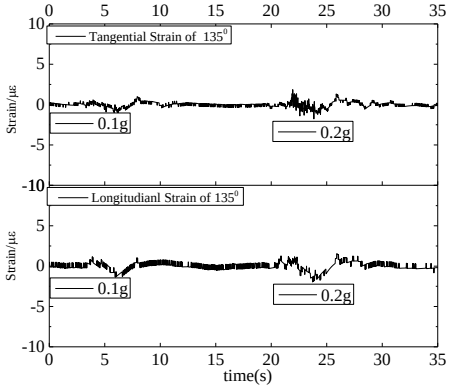

(b) hoop and longitudinal strain in 135°

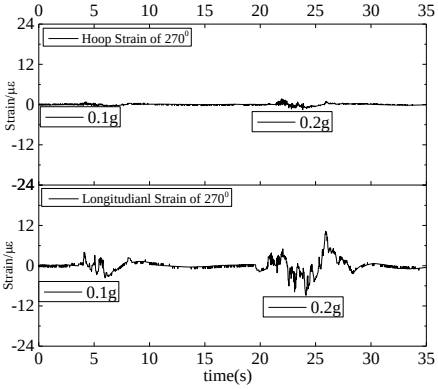

(c) hoop and longitudinal strain in 270°

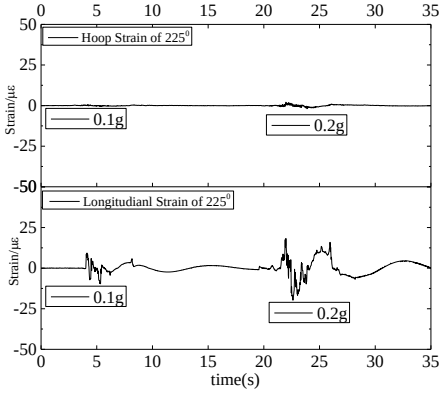

(d) hoop and longitudinal strain in 225°

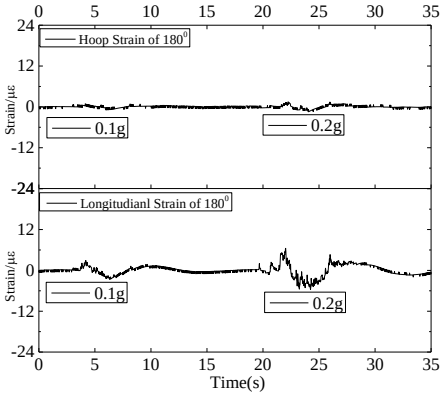

(e) hoop and longitudinal strain in 180°

Fig. 15 hoop and longitudinal Strain in *X*-direction of the Section # 1

Fig. 16 shows the maximum longitudinal and hoop strains at the inner and outer surfaces of the tunnel under excitation in the *X* direction (i.e., for events EQ2, EQ4 and EQ5). The deformation characteristics of the tunnel model are described using the absolute maximum strain in the longitudinal and hoop direction. The tension strain and compression strain are used to describe the strain of the model tunnel, the negative strain represents the compression of the model tunnel, the positive strain represents the tension of the model tunnel.

Figs. 16(a) and (c) show the longitudinal strain at the outer and inner surface the model tunnel, respectively. At the small peak of the input acceleration, the longitudinal strain of the model tunnel is in tension and less than 5 $\mu\varepsilon$, as the peak acceleration of input motion increases, the tension strain gradually increases, the maximum tension strain of inner and outer surface of the model tunnel are located at the 225^o and 270^o of the model tunnel, respectively.

Figs. 16(b) and (d) show the hoop strain of the outer and inner surface of the model tunnel with different peak accelerations. When the peak acceleration of input motion is 0.1 g, the hoop strain of the model tunnel is in tension and is less than 10 $\mu\varepsilon$, with the increasing of peak acceleration, the model tunnel is in tension. The maximum deformation of the hoop strain is located in a conjugate of the model tunnel at 45^o

The deformation of the tunnel can be strongly influenced by the ground deformation. Under the ground motion, the ground deformation developed from underground to the ground surface, as shown in Fig. 14. The

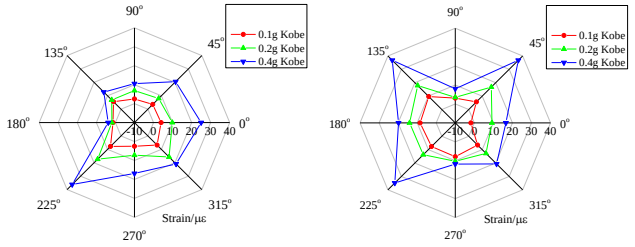

(a) Inner surface of the tunnel longitudinal (b) Inner surface of the tunnel hoop

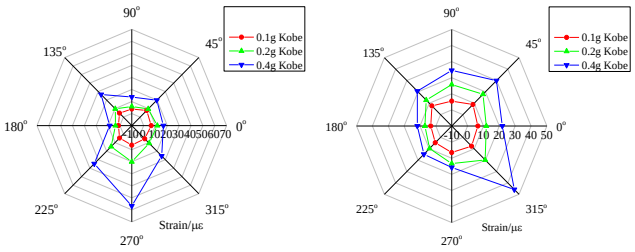

(c) Outer surface of the tunnel longitudinal (d) Outer surface of the tunnel hoop

Fig. 16 Maximum strains of the model tunnel with different peak accelerations

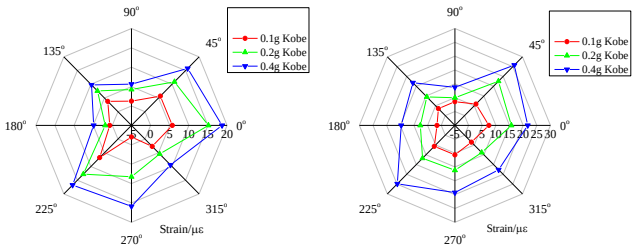

(a) Inner surface of the tunnel longitudinal (b) Inner surface of the tunnel hoop

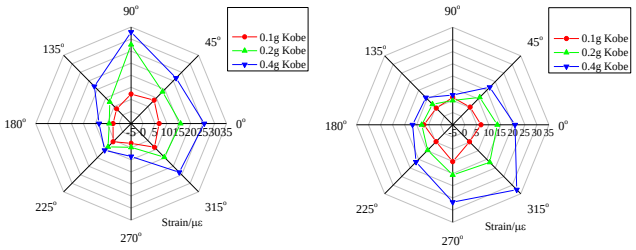

(c) Outer surface of the tunnel longitudinal (d) Outer surface of the tunnel hoop

Fig. 17 Maximum strains of the model tunnel with SAL

Table 6 maximum strain of the model tunnel with SAL and without

Maximum Strain ($\mu\varepsilon$)		Model tunnel	Model Tunnel with SAL	Reduction factor $=(S_T-S_{SAL})/S_T$
Longitudinal	Inner surface	36.21	18.69	48.39%
	Outer surface	56.78	32.69	42.43%
Hoop	Inner surface	36.77	25.78	29.99%
	Outer surface	45.80	32.65	28.72%

S_{SAL} is the strain of the model tunnel with SAL; S_T is the strain of the model tunnel

development of shear strain in the sand due to base excitation caused a shear force at the tunnel, the why the hoop deformation of the tunnel is in the 45° conjugate angle under excitation in the *Y* direction.

3.5 Effect of the SAL on the tunnel strains development

Fig. 17 shows the maximum longitudinal and hoop strains at the inner and outer surfaces of the model tunnel with the SAL under excitation in the *X* direction for events EQ2, EQ4 and EQ5.

Figs. 17(a) and (c) show the longitudinal strain at the outer and inner surface the model tunnel, respectively. As can be seen, as the peak acceleration of input motion increases, the tension strain gradually increases. However, the maximum tension strain of inner and outer surface of the model tunnel are smaller compared to that of model tunnel without SAL. Similar finding can be observed when the hoop strain is considered Figs. 17(b) and (d).

The maximum strain of the model tunnel with SAL and without were summarized in Table 6, in view of difference of the strain of the model tunnel, the reduction factor of the SAL is calculated. In the main *X* excitation, the longitudinal strain of the model tunnel with the SAL can be 40% smaller than that of the model tunnel without the SAL. For the hoop strain of the model tunnel with the SAL can reduced for more than 25% compared to the model tunnel without the SAL.

3.6 Soil-structure interaction

In this study, the soil-structure interaction is investigated through the dynamic earth pressure between the model tunnel and the sand. The dynamic earth pressure cells have measured the dynamic earth pressures at four symmetrical points of the tunnel (see Fig. 6(b)).

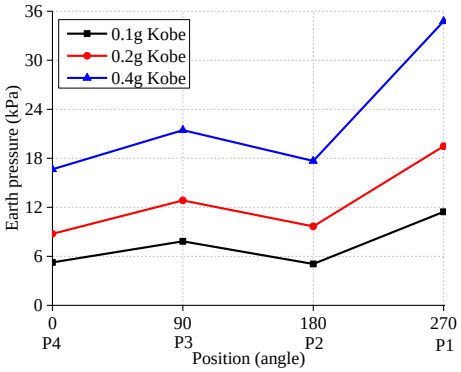

Fig. 18 Maximum earth pressure distribution on soil-structure interface

Fig. 18 shows the maximum dynamic earth pressures of the model tunnel for events EQ2, EQ4 and EQ5. As can be seen, as the peak accelerations of input motion increases, the earth pressure also increases, the maximum earth pressure took place at the bottom of the model tunnel. The

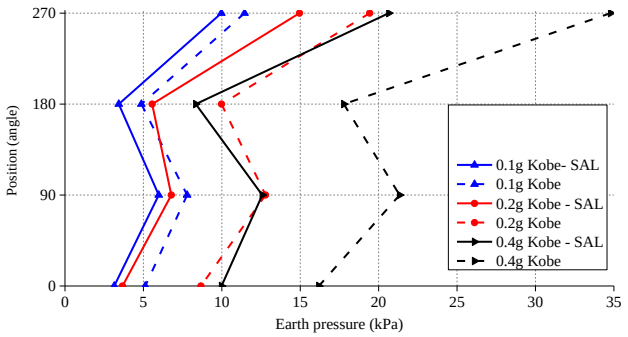

Fig. 19 Comparison of maximum earth pressure with the SAL

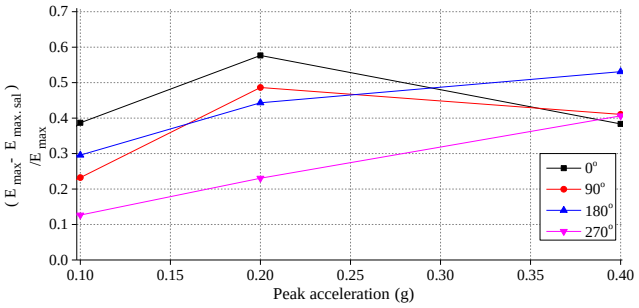

Fig. 20 SAL reduction factor

earth pressures at the left and the right side of the tunnel are lower as compared with those at the other positions.

Fig. 19 shows a comparison of the maximum dynamic earth pressures of the model tunnel with and without the SAL under the excitation of EQ2, EQ4, EQ5. As can be seen, the earth pressures of the tunnel with the SAL were lower than those of the tunnel without. Fig. 20 shows the reduction factor of the SAL on the dynamic earth pressure when subjected to excitation with different peak accelerations. The calculation of the reduction factor is shown in Eq. (2), it can be seen that the shock absorption effect of earth pressure with SAL changes for different position of the tunnel model. With a larger peak acceleration level, the reduction factor of SAL for the earth pressure is also increased. When considering a large peak acceleration excitation (i.e., 0.4 g), the reduction factor of the SAL is significant. The average reduction factor of the SAL is more than 35%.

$$\text{reduction factor} = \frac{\left(E_{\max} - E_{\max.sal}\right)}{E_{\max}} \tag{2}$$

$E_{\max}$ is the earth pressure of model tunnel without SAL; $E_{\max.sal}$ is the earth pressure of model tunnel with SAL.

4. Conclusions

This paper presented experimental results obtained from a series of shake table tests on a circle model tunnel embedded in compacted sand. A rigid soil container filled with sand was used. Using strain gauges, accelerometers and dynamic earth pressure cells, the dynamic response of the tunnel during shake table experiment were measured. The dynamic response of the tunnel linings with and without the SAL material have also been compared and analyzed. From the results, it can be seen that:

- Due to the weight of model tunnel and the difference of wave propagation in the macro concrete and sand, the acceleration in the *X* direction at the crown of model tunnel is higher with respect to the acceleration of the soil at the same burial depth.
- The SAL can reduce the acceleration of model tunnel. At a larger peak accelerations (i.e., 0.2 g and 0.4 g), the peak acceleration of the model tunnel with the SAL is half of that of the tunnel without.
- The hoop deformation of model tunnel is in tension. With a larger peak acceleration, the hoop deformation increases. The position of maximum deformation of model tunnel is in 45° conjugate angle.
- Based on the reduction factor due to the SAL on the hoop deformation of the model tunnel, it is shown that the SAL can reduce the tensile strain on a tunnel for up to 40%. With SAL, the hoop strain can also be reduced for about 25%.
- The maximum earth pressure took place at the bottom of the model tunnel. The earth pressure at the crown of model tunnel is higher than those on the side of the model tunnel.
- The SAL has can reduce the dynamic earth pressure on the tunnel model. For the different position of the model tunnel, the reduction factor of SAL is also different. This reduction can vary from 10% to 50%.

Acknowledgements

This research was supported by the China Railway Corporation Key Project (Grant No. 2014G010-G) and the National Engineering Laboratory for Construction Technology of High Speed Railway. All supports are gratefully acknowledged.

References

Abuhajar, O., Naggar, EI.H. and Newson, T. (2015), "Seismic soil-culvert interaction", *Can. Geotech. J.*, **52**, 1-19.

Andrew, D.G. (1997), "Physical scale model of geotechnical structure at one-g", Ph.D. Dissertation, California institute of Technology Pasadena, California, USA.

Bhattacharya, S., Muralikrishna, A., Lombardi, D., Crewe, A. and Alexander, N. (2012), "Economic MEMS based3-axis water proof accelerometer for dynamic geo-engineering applications", *Soil Dyn. Earthq. Eng.*, **36**, 111-118.

Chen, Z.Y. and Shen, H. (2014), "Dynamic centrifuge tests on isolation mechanism of tunnels subjected to seismic shaking", *Tunnel. Underg. Space Technol.*, **42**, 67-77.

Cilingir, U. and Madabhushi, S.P.G. (2011), "Effect of depth on the seismic response of square tunnels", *Soil. Found.*, **51**(3), 449-457.

David, M.W., Adam, C. and Colin, T. (2002), "Shaking table testing of geotechnical models", *Int. J. Phys. Model. Geotechnol.*, **1**, 1-13.

Fishman, K.L., Mander, J.B. and Richards, R. Jr. (1995),

"Laboratory study of seismic free-field response of sand", *Soil Dyn. Earthq. Eng*., **14**, 33-43.
Giannakou, A., Nomikos, P., Anastasopoulos, I., Sofianos, A., Gazetas, G. and Yiouta-Mitra, P. (2005), "Seismic behaviour of tunnels in soft soil: parametric numerical study and investigation on the causes of failure of the Bolu Tunnel (Duzce, Turkey, 1999)", Eds. Yücel Erdem and Tülin Solak, Underground Space Use: Analysis of the Past and Lessons for the Future, Taylor & Francis Group, London.
Ha, I.S., Olson, S.M., Seo, M. and Kim, M. (2011), "Evaluation of reliquefaction resistance using shaking table tests", *Soil Dyn. Earthq. Eng.*, **31**, 682-691.
Hashash, Y.M.A., Hook, J.J., Schmidt, B. and Yao, J.I.C. (2001), "Seismic design and analysis of underground structures", *Tunnel. Underg. Space Technol.*, **16**(2), 247-293.
Hassan, S., Alexander, K., Youssef, M.A., Hashash, B., Anoosh, S. and Alex, K. (2009), "Contact interface in seismic analysis of circular tunnels", *Tunnel. Underg. Space Technol*., **24**, 482-490.
Hessabi, R.M., Merican, O. and Ozturk, B. (2017), "Exploring the effects of tuned mass dampers on the seismic performance of structures with nonlinear base isolation systems", *Earthq. Struct.*, **12**(3), 286-296.
Hou, S., Tao, L.J., Li, S.L. and Wu, B.L. (2014), "Shaking table test for dynamic response in portal section of mountain tunnel with shock absorption layer", *World Earthq. Eng.*, **30**(3), 187-195.
Huang, M., Liu, M.Q. and Gao, B. (2011), "Research of similar guidelines and parameters for tunnel seismic model test", *Technol. Econ. Area. Commun*., **64**(2), 64-66.
ISO 23469 (2005), Bases for Design of Structures-Seismic Actions for Designing Geotechnical Works, ISO International Standard.
Jiang, L., Chen, J. and Li, J. (2010), "Seismic response of underground utility tunnels: shaking table testing and FEM analysis", *Earthq. Eng. Eng. Vib*., **9**(4), 555-567.
Kusakabe, O., Takemura, J., Takahashi, A., Izawa, J. and Shibayama, S. (2008), "Physical modeling of seismic responses of underground structures", *Proceedings of the Twelfth International Conference of International Association for Computer Methods and Advances in Geomechanics*, Goa, India, July.
Lanzano, G. (2009), "Physical and analytical modeling of tunnels under dynamic loadings", Ph.D. Dissertation, University of Naples, Italy.
Lanzano, G., Bilotta, E., Russo, G., Silvestri, F. and Madabhushi, S.P.G. (2012), "Centrifuge modeling of seismic loading on tunnels in sand", *Geotech. Test. J*., **35**(6), 854-869.
Lombardi, D., bhattacharya, S., Scarpa, F. and Biabchi, M. (2015), "Dynamic response of a geotechnical rigid model container with absorbing boundaries", *Soil Dyn. Earthq. Eng.*, **69**, 46-56.
Milanchian, R., Hosseini, M. and Nekooei, M. (2017), "Vertical isolation of a structure based on different states of seismic performance", *Earthq. Struct.*, **13**(2), 103-118.
Mizuno, H. and Iiba, M. (1984), "Shaking table testing of seismic building-pile-soil interaction", *Proceedings of the 8th World Conference on Earthquake Engineering*, San Francisco, USA, May.
Patil, S.J., Reddy, G.R., Shivshankar, R., Babu, R., Jayalekshmi, B.R. and Kumar, B. (2016), "Seismic base isolation for structures using river sand", *Earthq. Struct.*, **10**(4), 829-847.
Penzien, J. (2000), "Seismically induced racking of tunnel linings", *Earthq. Eng. Struct. Dyn.*, **29**, 683-691.
Qin, X. (2016), "Experimental studies of structure- foundation - soil interaction effect on upliftable structure", PhD. Thesis, University of Auckland, Auckland, New Zealand.
Qin, X. and Chouw, N. (2017), "Shake table study on the effect of mainshock-aftershock sequences on structures with SFSI", *Shock and Vibration*, **2017**, Article ID 9850915, 12.
Qin, X. and Chouw, N. (2018), "Response of structure with controlled uplift using footing weight", *Earthq. Struct.*, **15**(5), 555-564.
Shen, Y.S., Gao,B., Yang, X.M. and Tao, S.J. (2014), "Seismic damage mechanism and dynamic deformation characteristic analysis of mountain tunnel after Wenchuan earthquake", *Eng. Geol.*, **180**, 85-98.
Tao, L.J., Li, S.L., Hou, S. and Wu, B.L. (2016), "Shaking table test for seismic response in portal section of mountain tunnel", *World Earthq. Eng.*, **32**(4), 7-16.
Tavakoli, H.R., Naghavi, F. and Goltabar, A.R. (2015), "Effect of base isolation systems on increasing the resistance of structures subjected to progressive collapse", *Earthq. Struct.*, **9**(3), 639-656.
Tsinidis, G., Heron, C., Pitilakis, K. and Madabhushi, G.S.P. (2014), "Physical modeling for the evaluation of the seismic behavior of square tunnels", *Seismic Eval. Rehab. Struct.*, **26**, 389-406.
Tsinidis, G., Heron, C., Pitilakis, K. and Madabhushi, S.P.G. (2015), "Centrifuge modeling of the dynamic behavior of square tunnels in sand", *Geol. Earthq. Eng.*, **35**, 509-523.
Vasiliadis, L.K. (2016), "Seismic evaluation and retrofitting of reinforced concrete buildings with base isolation systems", *Earthq. Struct.*, **10**(2), 293-311.
Victor, A.C. (2010), "Scale model shake table testing of underground structures in soft clay", Master Degree Thesis, California Polytechnic State University, USA.
Wang, J.N. (1993), "Seismic design of tunnels A simple state-of-the-art design approach", Monograph 7, Parsons Brinckerhoff, New York, NY, USA.
Wei, B., Wang, P., He, X.H., Zhang, Z. and Chen, L. (2017), "Effects of friction variability on a rolling-damper-spring isolation system", *Earthq. Struct.*, **13**(6), 551-559.
Whitman, R.V. and Lambe, P.C. (1986), "Effect of boundary conditions upon centrifuge experiments using ground motion simulation", *Geotech. Test. J.*, **9**(2), 61-71.
Yamada, T., Nagatani, H., Ohbo, N., Izawa, J., Shigesada, H. and Kusakabe, O. (2004), "Seismic performance of flat cross-sectional tunnel with countermeasures", *Proceedings of the 13th World Conference on Earthquake Engineering*, Prentice-Hall, London, UK, October.
Zhou, X.J., Hu, H.Y., Jiang, B., Zhou, Y.F. and Zhu, Y. (2016), "Numerical analysis on stability of express railway tunnel portal", *Struct. Eng. Mech.*, **57**(1), 1-20.

KT